Structure of a type III secretion needle at 7-Å resolution provides insights into its assembly and signaling mechanisms

Takashi Fujii[a], Martin Cheung[b], Amandine Blanco[b], Takayuki Kato[a], Ariel J. Blocker[b,1], and Keiichi Namba[a,c,1]

[a]Graduate School of Frontier Biosciences, Osaka University, 1-3 Yamadaoka, Suita, Osaka 565-0871, Japan; [b]Schools of Cellular and Molecular Medicine and Biochemistry, Medical Sciences Building, University of Bristol, University Walk, Bristol BS8 1TD, United Kingdom; and [c]Riken Quantitative Biology Center, 1-3 Yamadaoka, Suita, Osaka 565-0871, Japan

Edited by David DeRosier, Brandeis University, Waltham, MA, and approved January 9, 2012 (received for review October 4, 2011)

Type III secretion systems of Gram-negative bacteria form injection devices that deliver effector proteins into eukaryotic cells during infection. They span both bacterial membranes and the extracellular space to connect with the host cell plasma membrane. Their extracellular portion is a needle-like, hollow tube that serves as a secretion conduit for effector proteins. The needle of *Shigella flexneri* is approximately 50-nm long and 7-nm thick and is made by the helical assembly of one protein, MxiH. We provide a 7-Å resolution 3D image reconstruction of the *Shigella* needle by electron cryomicroscopy, which resolves α-helices and a β-hairpin that has never been observed in the crystal and solution structures of needle proteins, including MxiH. An atomic model of the needle based on the 3D-density map, in comparison with that of the bacterial-flagellar filament, provides insights into how such a thin tubular structure is stably assembled by intricate intermolecular interactions. The map also illuminates how the needle-length control protein functions as a ruler within the central channel during export of MxiH for assembly at the distal end of the needle, and how the secretion-activation signal may be transduced through a conformational change of the needle upon host-cell contact.

helical image analysis | Shigella pathogenesis | bacterial protein secretion

Type III secretion systems (T3SSs) are found in many Gram-negative bacteria, forming injection devices to deliver bacterial effector proteins into eukaryotic host cells during infection (1). Understanding the 3D structure of T3SSs is therefore important for the design of new broad-spectrum strategies to combat bacterial pathogens. These macromolecular assemblies are composed of approximately 25 proteins and span the bacterial cytoplasm, membranes, and the extracellular space to connect with the host-cell plasma membrane. As they are genetically and morphologically related to bacterial flagellar basal bodies (FBBs), functional parallels with that system have been drawn (2). However, FBBs are constitutively active in sequential secretion of axial flagellar proteins, whereas T3SS activation for secretion requires physical contact with host cells. The major extracellular portion of T3SSs is an approximately 50-nm-long, hollow needle-like structure, serving as a secretion conduit for effectors. The needle is made by the helical assembly of a single, small and conserved protein (3, 4). It has been shown that the needle protein, MxiH in the enteropathogenic species *Shigella*, is directly involved in transducing the signal of host-cell contact to the base of the apparatus (5).

Shigella flexneri, the agent of human bacillary dysentery, uses a T3SS for invasion of, and dissemination within, the gut-epithelial lining (6). Its T3SS is made up of three parts (7): a cytoplasmic portion, a transmembrane region, and the extracellular "needle." The inner-membrane region houses the export apparatus, which connects to the periplasmic end of the needle, itself held within the central cavity of an outer-membrane secretin (8). The secreted proteins pass into the host cell via a translocation pore assembled from the tip of the needle into the host membrane (7).

Within the *Shigella* needle, MxiH is arranged into a helical polymer that shares packing parameters with the bacterial flagellar filament (4). The needle is topped by a "tip complex," which is most likely the host-cell sensor and eventually forms the translocation pore (9). Point mutations in the needle protein lead to deregulated secretion as well as compositionally and functionally altered tips (5, 9, 10). Following discovery that short C-terminal deletions prevent MxiH polymerization, partial crystal and NMR structures from several species revealed a helix-turn-helix hairpin fold (11–13) (Fig. S1). In all these, the terminal half of the N-terminal α-helix is unstructured and invisible to various degrees. Using a 16-Å resolution 3D-image reconstruction of the needle from negative-stain EM images (4), a pseudoatomic model of the needle was generated (12). However, neither this nor EM analysis of the helical parameters of deregulated mutants (14) revealed how the needle controls secretion. The recent electron cryomicroscopy (cryo-EM) image reconstruction of the *Salmonella* needle did not reveal the structural architecture in detail either, due to its limited resolution (15). Despite the knowledge accumulated, the detailed needle architecture and hence its mechanisms of assembly and function remain unknown.

Here we provide a 7-Å resolution 3D-image reconstruction of the MxiH needle by cryo-EM. The density map resolves secondary structures such as α-helices and β-strands, directly visualizing a β-hairpin not present in the crystal structure (12). An atomic model based on the map provides insight into how the thin tubular structure is stably assembled and how the needle-length control protein functions as a ruler within the central channel during the export of MxiH for its assembly at the growing, distal end of the needle. The model also sheds light on how the secretion activation signal may be transduced from the tip of the needle to the inner membrane export apparatus.

Results

Cryo-EM Image Reconstruction of Wild-Type Needles. We sought to obtain a high-resolution structure of the needle using cryo-EM. However, the needle diameter is only 7 nm and its subunit just

Author contributions: T.F., A.J.B., and K.N. designed research; T.F., M.C., A.B., A.J.B., and K.N. performed research; T.K. set up and maintained the cryoelectron microscopy and computation facilities for high-quality imaging and analysis; T.F., M.C., A.B., A.J.B., and K.N. analyzed data; and T.F., M.C., A.J.B., and K.N. wrote the paper.

The authors declare no conflict of interest.

This article is a PNAS Direct Submission.

Freely available online through the PNAS open access option.

Data deposition: The atomic coordinates of a 22-mer needle model have been deposited in the Protein Data Bank, www.pdb.org (PDB ID code 3J0R). The electron density map has been deposited in the Electron Microscopy Data Bank, http://www.emdatabank.org/ (EMDB code EMD-5352).

[1]To whom correspondence may be addressed. E-mail: keiichi@fbs.osaka-u.ac.jp or ariel.blocker@bris.ac.uk.

This article contains supporting information online at www.pnas.org/lookup/suppl/doi:10.1073/pnas.1116126109/-/DCSupplemental.

9 kDa, making image contrast of frozen-hydrated specimens in vitreous ice extremely poor and therefore accurate image alignment for high-resolution analysis difficult. To surmount this, we made methodological improvements (16, 17) to obtain higher image contrast (Fig. 1*A*). We used an electron cryomicroscope, JEM-3200FSC (JEOL), equipped with a field-emission electron gun, a liquid helium-cooled specimen stage, an Ω-type in-column energy filter, and a 4,096 × 4,096 CCD camera, to collect cryo-EM images of purified needles, made artificially long by MxiH overexpression and then sheared off the bacterial surface and into smaller (approximately 300 nm) fragments. We operated the electron microscope at an accelerating voltage of 200 kV, and collected images at specimen temperatures of around 50 K. We collected cryo-EM images of wild-type needle from approximately 300 CCD frames, carried out helical image reconstruction using approximately 100,000 needle segments (Table 1), and obtained the structure at 7.7-Å resolution (based on the Fourier shell correlation = 0.5 criterion; Fig. S2). The 3D-density map is shown in stereoview in Fig. 1*B*. The image processing statistics are given in Table 1. The average of power spectra of all the image segments used for 3D-image reconstruction shows sharp layer lines (Fig. S3), indicating the high homogeneity of the needle structure.

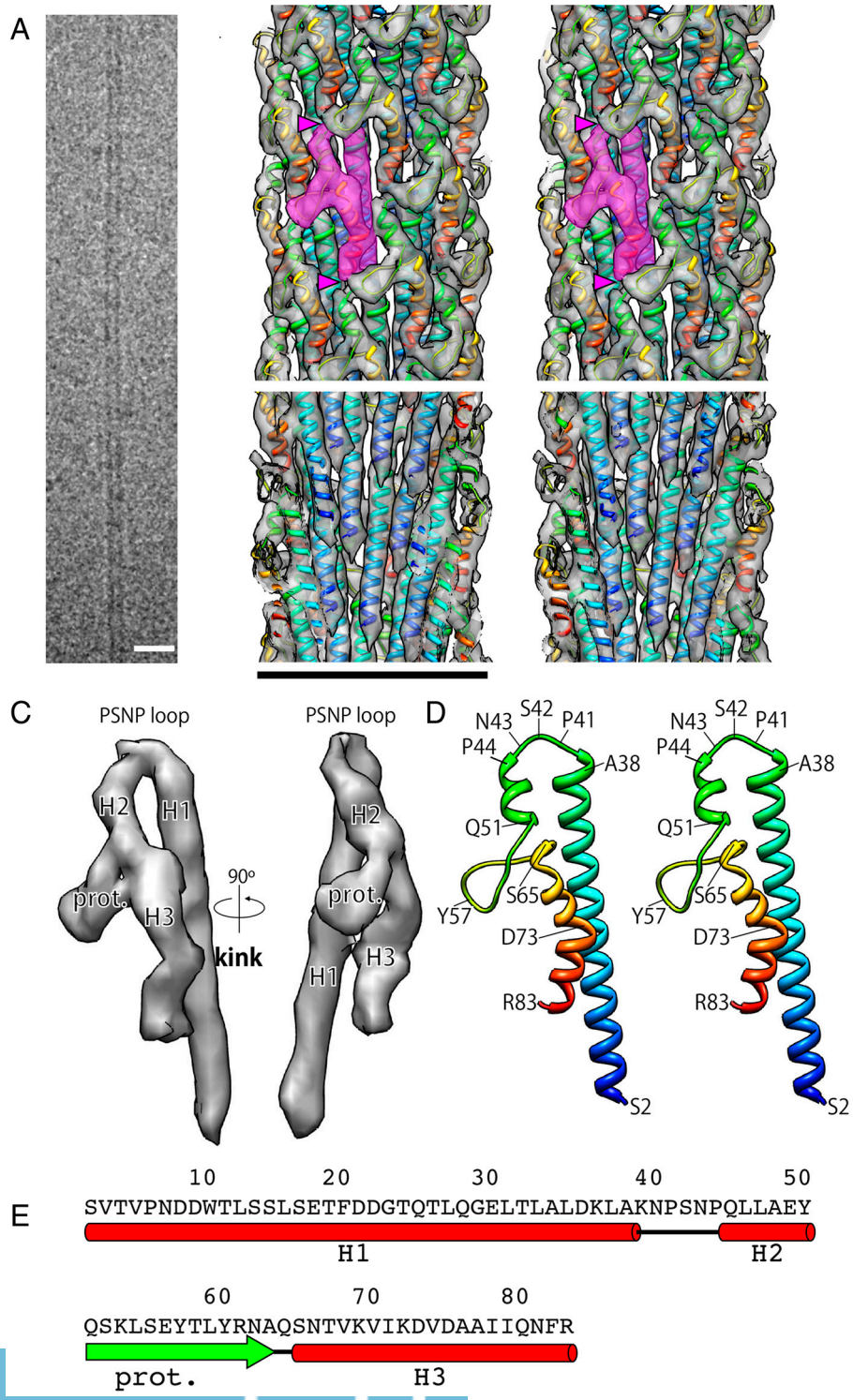

Fig. 1. CryoEM image, reconstruction and model of MxiH needle. (*A*) Individual filament from electron micrograph used in analysis. (Scale bar: 20 nm.) (*B*) 3D-density map of the needle with fitted atomic model in stereo. The outer surface (*Upper*) and the inner surface of the half-cut needle (*Lower*) are shown. One MxiH molecule is colored in magenta; the *Upper* of the two arrowheads indicates where the β-hairpin from a neighboring subunit in the 6-start helix contacts the head of the molecule in magenta and the *Lower* one indicates where the C terminus of the molecule in magenta contacts the head of the subunit below it within its 11-start protofilament. (Scale bar: 7 nm.) (*C*) Two different views of the surface representation of an individual protomer rotated by 90° (H1, H2, and H3 indicate the position of α-helices, "prot" that of the protrusion between H2 and H3, and "kink" that of a bend in H3 at the level of D73). (*D*) Stereoview of the individual MxiH model. The chain is color coded from blue to red, going through the rainbow colors, from the N terminus to the C terminus. (*E*) The amino acid sequence of MxiH with secondary structures identified in the model.

Table 1. Image-processing statistics

	WT	D73A	Q51
Number of micrographs	330	380	330
Total number of segmented images in initial selection	98,853	59,692	59,795
Total number of segmented images used in final map	64,583	37,377	36,738
The number of asymmetric units	252,324	146,031	143,534
Resolution (FSC = 0.143)	6.2 Å	6.8 Å	7.6 Å
Resolution (FSC = 0.5)	7.7 Å	7.7 Å	8.3 Å

FSC, Fourier shell correlation.

The density map clearly resolved α-helices as rod-like densities (Fig. 1*B*). The refined helical parameters are 4.30 Å for the axial rise and 64.1° for the azimuthal rotation along the 1-start helix (Table 2) confirming previous data (4, 14). However, none of the available atomic models of MxiH and its homologs (Fig. S1) (12, 13, 18, 19) can be fitted into our density map.

Initial Remodeling of the Needle Protein. Because the 3D map allowed the identification of correspondences with secondary structural elements of the MxiH crystal structure, we tried to fit the MxiH "head" (residues 26–51), including the short Pro-Ser-Asn-Pro (PSNP; residues 41–44) loop into the map. The conformation of this portion is nearly the same in all the NMR and X-ray structures of monomeric proteins available for this protein family (12, 13, 18, 19) (Fig. S1). Indeed, the head motif fitted well into the map. The head portion has two ends. One extends toward the central channel, forming a long rod-shaped density labeled H1 (Fig. 1*C*). The other forms the external surface of the needle structure and includes two rod-shaped densities labeled H2 and H3 and a "protrusion" between them (Fig. 1*C*). Given their size and shape the H1, H2, and H3 densities were modeled as α-helices in Fig. 1*D*. H1 is approximately 60-Å long, corresponding to an α-helix of approximately 40 residues, which is in good agreement with the full-length N-terminal helix extended from the MxiH crystal structure (12). This fact led us to assign H1 to the N-terminal half and H2 and H3 to the C-terminal half of MxiH.

Experimental Validation of the Model. To confirm this assignment, we examined the effect of termini alterations. In the 3D map, H3 of one subunit interacts with the head of the subunit immediately below (Fig. 1*B*, *Upper*, pink arrowhead) whereas its H1 lies free (Figs. 1*B*, *Lower*, and 2*A*), suggesting that the C terminus plays a more critical role than the N terminus for needle formation. It has been shown that three to five residue deletions at the MxiH C terminus cause absolute polymerization defects, implying that this region is directly involved in the intermolecular interactions for polymerization (5). The five C-terminal residues of *Salmonella* MxiH homolog PrgI are essential for T3SS function whereas its six N-terminal residues are dispensable (13). Removal of any number of MxiH N-terminal residues beyond three generated a null phenotype (Fig. S4). Therefore, we generated shorter MxiH truncations and extensions (duplications of the first and last three residues; Fig. 3). We tested for T3SS assembly by examining overnight secretion of early-acting virulence proteins into the culture medium and for T3SS functionality using an artificial inducer of secretion, the small amphipathic dye Congo red (CR) (5). CΔ1 was still partially functional for needle assembly and T3SS activation, but CΔ2, CΔ3, and C + 3 were not (Fig. 3 *A* and *B* and Fig. S5). In contrast, NΔ2 and NΔ3 still allowed needle formation, but only NΔ2 permitted substantial T3SS activation (Fig. 3 *A* and *B*) although it led to unstable polymers. N + 3 allowed better than normal MxiH secretion (Fig. S5) and polymerization (Fig. 3*A*) although it displayed reduced sensitivity to CR (Fig. 3*B*). In the N + 3 needle cryo-EM image reconstruction, the extension was invisible and hence probably disordered. However, because the MxiH N terminus tolerates more substantial modifications than its C terminus, H1 extending into the central channel must be N terminal and H2 and H3 C terminal.

Table 2. Helical parameters of the wild type and two mutants

Genotype	Translation, Å	Rotation, °
Wild type	4.30	64.06
D73A	4.33	64.03
Q51A	4.24	64.04

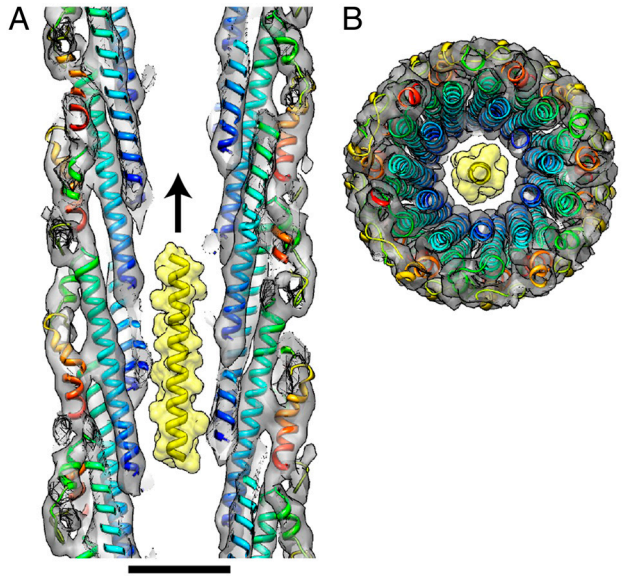

Fig. 2. Size of the needle channel and an α-helical peptide as a model secretion substrate. (*A*) Side view of the axial section, and (*B*) top view of the cross section showing the needle channel. The peptide shown in yellow is $MxiH_{3–37}$. (Scale bar: 20 Å.)

Refinement of the Model. Given previous sequence analysis suggesting the presence of a β-structure for residues L54–S65 (5, 13), the protrusion between H2 and H3 can be interpreted as a β-hairpin. We therefore built a preliminary atomic model of MxiH with-

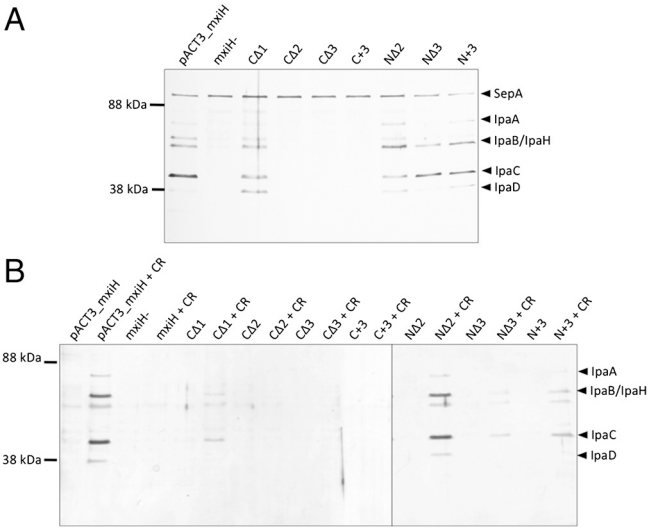

Fig. 3. Validation of subunit orientation by analysis of secretion in MxiH deletion mutants. C- or N-terminal amino acid deletions (Δ) or duplications (+) were cloned into pACT3 and transformed in mxiH$^-$ *Shigella*. *A*) Ipa protein "leakage" into the culture supernatant after overnight culture (proteins are indicated on the right; the auto-transporter-secreted SepA acts as a loading control). *B*) Congo red induction assays as visualized by SDS-PAGE and Silver staining. Molecular weights are indicated on the left.

in the needle using the A-form of the MxiH crystal structure for residues G21-Y50 as the head. Then, the N-terminal α-helix was extended from the head to S2, and the β-hairpin (Q51–Q64) and C-terminal α-helix (S65–R83) were built based on the map. Because there are heptad repeats in both the N- and C-terminal regions, we placed the three α-helices with their hydrophobic residues facing to each other as should occur in an α-helical coiled-coil structure and optimized the model as described in *SI Materials and Methods*.

Structures of Mutant Needles Deregulated for Secretion. To advance our understanding of how the needle acts to transduce the signal of host-cell contact, we examined the structures of needles purified from strains overexpressing either of two key needle protein mutants, D73A and Q51A (Fig. 4), which we have previously characterized as having altered-tip-complex composition and deregulated secretion (5, 9). These mutants were selected because they show the highest needle stability and order amongst all those previously analyzed (14). MxiH(D73A) lacks the tip complex, secretes early-virulence proteins constitutively, and is uninducible by CR. MxiH(Q51A) displays minor alterations in composition of the tip complex, is constitutively active for secretion, and is still inducible by CR.

We carried out cryo-EM helical-image reconstruction of these two mutant needles and obtained the density maps at 7.7- and 8.3-Å resolution, respectively (based on the Fourier shell correlation = 0.5 criterion; Fig. S2). As shown in Table 2 the refined helical parameters are identical to those of wild-type, confirming previous data (4, 14). Comparison of the wild type, D73A, and Q51A mutant needles (Fig. 5) revealed that the structures are also nearly identical and that no significant structural change is observed. Given that they are independent reconstructions, their similarity demonstrates the reproducibility of the structural analysis performed. The results suggest that any structural changes in the needle protein responsible for the functional alteration are either too small to detect at the present resolution or not retained in needles isolated from their base and tip.

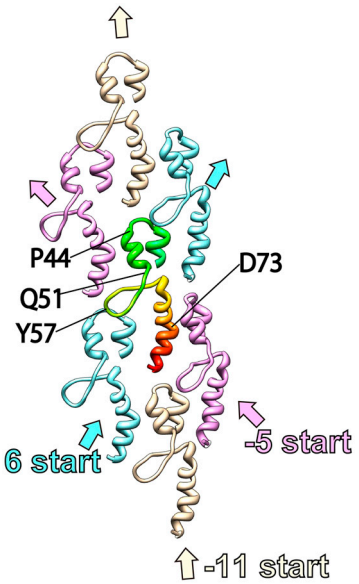

Fig. 4. Mapping of four residues (P44, Q51, Y57, and D73) and the intermolecular interactions along each helical line. Seven MxiH subunits, each with the head loop and C-terminal chain, are shown in the side view of the outer surface of the needle with its axis vertical. The three major helical lines are indicated by three different colors with arrows indicating their directions. The central MxiH subunit, where key residues are indicated, is rainbow colored as in Fig. 1*D*. The neighboring subunits along the −5-start helix are colored pink, those along the 6 start are colored blue, and those along −11 start are colored beige.

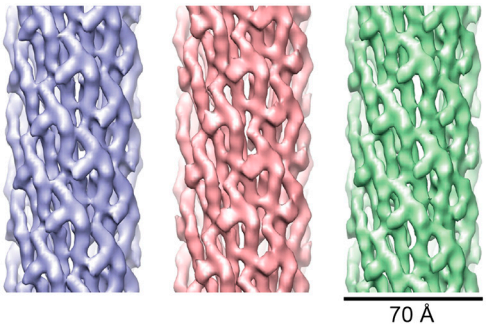

Fig. 5. 3D-image reconstructions of the wild-type and mutant needles. The 3D maps are shown for the needles from WT (*Left*, purple), D73A (*Center*, pink), and Q51A (*Right*, light green). The maps are presented at the same resolution to show the reproducibility of image analysis and any structural differences. To unify the resolution, a B factor of −220 Å^2 was applied to their structure factors using the cosine edge mask with a radius of 7.93 Å, which is the mean value of the Fourier shell correlation (FSC) for $FSC_{0.143}$ and $FSC_{0.5}$ of the Q51A mutant reconstruction, the worst of the three.

Discussion

The high-resolution T3SS needle structures described and validated herein have important implications for the understanding of protein polymers in general and of T3SS assembly and function in particular.

Refolding of Needle Proteins During Polymerization. The structures of the wild-type and two mutant needles presented here reveal a previously undescribed fold of the needle protein that is distinct from those previously seen in X-ray crystal structures and NMR solution structures. Using FTIR of the *Salmonella typhimurium* needle protein (PrgI*), soluble or polymerized into needles, as well as solid state nuclear magnetic resonance (ssNMR) of the latter, Poyraz et al. provided evidence for a change in secondary structure from α-helix to β-structure within the C-terminal region upon polymerization (13). The present structure identifies the precise region involved as the β-hairpin made of residues Q51–Q64, which overlaps well with the prediction of sequence analysis (5). Relatively small proteins without an extensive hydrophobic core can fold into different conformations depending on chemical and physical environments as well as upon assembly into larger structures. Therefore, it is not completely unexpected that MxiH, which is only 85 residues long, refolds upon assembly into the needle structure. The result shown here illustrates why caution should be exercised in interpreting the crystal structure of small monomeric proteins that normally function in assembled complexes.

Needle Stability. The model confirms that the needle structure corresponds to only the innermost tube of the flagellum (4, 17, 20, 21). What makes a tubular filament as thin as the needle so stable? The innermost tubes of the flagellar-axial structures are consolidated by interactions between coiled-coils of the D0 domain of their subunits but H2 and H3 are not so closely associated between neighboring needle subunits. However, the β-hairpin lies at the interface of subunits along all major three helical lines (6, −5, and −11 start; Fig. 4), perhaps working like a "linchpin" to stabilize the structure. To test this, we altered, shortened, or removed the β-hairpin by mutagenesis (Table S1). These mutants displayed poor MxiH expression or intrabacterial stability, very reduced secretion, and lack of needle assembly (Table S2). Interestingly, the mutated region corresponds to a portion of the *Pseudomonas* and *Yersinia* needle proteins known to interact tightly with their intracellular chaperone PscG/YscG in an extended conformation, suggesting that a similar complex may also exist in *Shigella* even though the PscG/YscG analog(s) remains unidentified (22, 23). We then altered residues to alanine where the β-hairpin interacts in neighboring molecules, along the 6-start

helix where the head joins up with H1 and the PSNP loop (Table S1). These changes also led to reduced MxiH expression and/or secretion (Table S2), preventing examination of whether these residues are also important for assembly. However, a previously generated mutant, Y57A, is informative (5). Y57A is expressed and secreted but leads to a reduced number of needles that are shorter than wild type. In our model, Y57 is located at the tip of the β-hairpin and plays an important role in intersubunit interactions along the 6-start helix, stabilizing the association of adjacent protofilaments, which are near-axial arrays of subunits along the 11-start helical line (Fig. 4). Therefore, the model explains the high conservation of this residue.

Needle Assembly. In addition, the model allows us to propose a mechanism for needle polymerization. The polymerization of each external portion of the bacterial flagellum requires an "assembly cap." The filament cap is a flat pentameric structure with "legs" that rotates above the helically growing structures to aid selection of the insertion site for the next flagellin subunit. The cap also has a central cavity open to the outside to promote the refolding and binding of the approximately 50-kDa subunits to the appropriate location (24). Although initially proposed to exist (2), no assembly cap has been found for the T3SS needle. However, given its small size, the needle protein may not need a polymerization-promoting complex (11). In view of the β-hairpin structure found, we now propose that the assembly process is as follows. Each needle subunit is exported possibly with its N terminus first, where its secretion signal is located (25). The terminus of each subunit would then bind to one of the five possible insertion sites and integrate into the lining of the channel. Then, the folding of the β-hairpin would stabilize the subunit position within the needle sufficiently to allow its C terminus to fold on the outside of the structure. When the right needle length is reached and a ruler molecule is secreted, the secretion specificity is switched to tip complex components (26). The addition of the first tip-complex protein (IpaD) is then sufficient to halt needle elongation (13).

Needle Length Control. The structure also provides insight into needle-length control. Needle subunits, like axial-flagellar proteins, are exported by T3SS through the central channel of the growing structure and assemble at its distal end (27, 28). The lengths of the needle and the flagellar hook are both controlled by conserved ruler proteins (29, 30). In the absence of their rulers, extra-long needles and hooks are produced. Two models have been proposed to explain how the rulers work (30–33). In one model, polymer elongation is controlled by several ruler molecules passing stochastically through the growing structure, with subunits and rulers traveling alternatively in the channel (30, 31, 33). In the other model, one ruler molecule positioned inside the channel is stretched gradually during polymer assembly, where the ruler coexists with polymer proteins translocated through the channel (32). The ruler is thought to adopt an α-helical conformation inside the channel based on a linear correlation between ruler size and polymer length, with the polymer extending by 1.9 Å per ruler residue (29, 32), because the axial translation of C^{α} atoms between adjacent residues is approximately 1.5 Å in an α-helix and approximately 3.7 Å in an extended chain. The present structure shows that the channel diameter is approximately 13 Å (Fig. 2). Because the diameter of an α-helix is approximately 10 Å, it is impossible for a ruler and a polymer protein to coexist in the channel, ruling out the second model.

Transduction of the Host Cell Contact Signal. Does our density map help us understand how the needle transduces the host cell contact signal to the export apparatus? The four residues (P44 + Q51, Y57, and D73) that lead to an inability to transmit the activation signal when altered to alanine (5) lie in positions where they may directly (Y57 and Q51) or indirectly (P44 and D73) affect the orientation or conformation of the β-hairpin. The location of the MxiH β-hairpin is topologically analogous to that of the β-hairpin in domain D1 of flagellin in the flagellar filament (34). In flagellin, the β-hairpin is crucial to the polymorphic supercoiling of the filament, which involves a 0.8 Å change in the axial repeat along the 11-start protofilament, in response to a change in the direction of motor rotation (34). The comparison of the two protofilament conformations of the flagellar filament called L and R type has shown that the conformational change of flagellin involved in the polymorphic supercoiling of the filament is the switch in the orientation of the outer core domains relative to the invariant structure of the tubular assembly of the inner core domains (35). However, the axial repeat is unaltered in needle mutants leading to deregulated secretion (14), as confirmed by our cryo-EM image analysis here (Table 2) and the density maps of D73A and Q51A mutant needles did not reveal significant conformational changes compared to that of wild type (Fig. 5). Nevertheless, the present model of the needle suggests that H2, H3, and the β-hairpin on the outer surface can be displaced relative to the tightly packed H1 helices in the inner core (Fig. 1*B*), perhaps by a conformational change in the PSNP loop. Such a displacement could be caused by a change in the conformation of the tip complex upon host-cell contact. The tight packing of the H1 helices could provide a solid framework for the cooperative propagation of the host contact signal down to the base of the needle and eventually to the export apparatus to activate effector secretion into host cells without changing the repeat and helical symmetry of the needle structure, just as speculated previously (11). In addition, it is quite possible that such changes would not be preserved when needles are isolated from their base and tip during purification. To unveil the signal transduction mechanism, the necessary next step is the structural examination of wild-type and mutant needles that have retained their tip and base by cryo-EM image analysis.

Materials and Methods

The long needles for cryo-EM image analysis were produced by overexpressing MxiH and isolated as described elsewhere (14). Needles prepared in Bristol were shipped to Osaka on wet ice as ultracentrifuge pellet with 25 μL supernatant solution left to cover it. Samples were vitrified within 7–10 d of generation. Needle aliquots were spun at 100,000 × *g* for 15 min 4 °C. The storage solution was removed and needles were gently resuspended in 500 μL of fresh storage buffer. A 2.1 μL sample solution was applied onto a Quantifoil holey carbon molybdenum grid (R0.6/1.0; Quantifoil) and plunge-frozen into liquid ethane using a Vitrobot (FEI). The specimen was observed at temperatures of 50–60 K using a JEOL JEM3200FSC electron microscope equipped with a liquid-helium-cooled specimen stage, an Ω-type energy filter, and a field-emission electron gun operated at 200 kV. Zero energy-loss images, with a slit setting to remove electrons of an energy-loss larger than 10 eV, were recorded on a 4,096 × 4,096 15 μm/pixel slow-scan CCD camera, TemCam-F415MP (TVIPS), at a magnification of around 89,285×, a defocus range of 1.0–2.5 μm and an electron dose of approximately 20 electrons/$Å^2$. The magnification was calibrated by measuring the layer line spacing of 23.0 Å in the Fourier transform of images of tobacco mosaic virus mixed in the sample solution. Image processing and analysis was done using the iterative helical real-space refinement method (36). Further details are described in *SI Materials and Methods*. The EM map and a 22-mer needle model were deposited in the Electron Microscopy Data Bank and the Protein Data Bank under accession numbers EMD-5352 and 3J0R, respectively.

ACKNOWLEDGMENTS. We thank Susan Lea for discussions and Akio Kitao and Takahisa Ikegami for helpful advice on building the β-hairpin motif and interpreting NMR structures, respectively. We are indebted to Donald L.D. Caspar for detailed and transforming comments on the manuscript. Gordon Frazer is thanked for synthesis of most of the PCR products required for generating the short N-and C-terminal MxiH deletion mutants. T.F. was a Japan Society for the Promotion of Science research fellow. This work was supported by Grants-in-Aid of Scientific Research from the Japanese Ministry of Education, Culture, Sports, Science, and Technology Grant 16087207 and 21227006 (to K.N.), a studentship from the School of Cellular and Molecular Medicine, University of Bristol (C.M.), and Wellcome Trust project Grant 088231 (to A.J.B. and K.N.).

1. Cornelis GR (2006) The type III secretion injectisome. *Nat Rev Microbiol* 4:811–825.
2. Blocker A, Komoriya K, Aizawa S (2003) Type III secretion systems and bacterial flagella: Insights into their function from structural similarities. *Proc Natl Acad Sci USA* 100:3027–3030.
3. Blocker A, et al. (2001) Structure and composition of the Shigella flexneri "needle complex," a part of its type III secreton. *Mol Microbiol* 39:652–663.
4. Cordes FS, et al. (2003) Helical structure of the needle of the type III secretion system of Shigella flexneri. *J Biol Chem* 278:17103–17107.
5. Kenjale R, et al. (2005) The needle component of the type III secreton of Shigella regulates the activity of the secretion apparatus. *J Biol Chem* 280:42929–42937.
6. Schroeder GN, Hilbi H (2008) Molecular pathogenesis of *Shigella* spp: Controlling host cell signaling, invasion, and death by type III secretion. *Clin Microbiol Rev* 21:134–156.
7. Blocker A, et al. (1999) The tripartite type III secreton of Shigella flexneri inserts IpaB and IpaC into host membranes. *J Cell Biol* 147:683–693.
8. Hodgkinson JL, et al. (2009) Three-dimensional reconstruction of the *Shigella* T3SS transmembrane regions reveals 12-fold symmetry and novel features throughout. *Nat Struct Mol Biol* 16:477–485.
9. Veenendaal AK, et al. (2007) The type III secretion system needle tip complex mediates host cell sensing and translocon insertion. *Mol Microbiol* 63:1719–1730.
10. Torruellas J, Jackson MW, Pennock JW, Plano GV (2005) The Yersinia pestis type III secretion needle plays a role in the regulation of Yop secretion. *Mol Microbiol* 57:1719–1733.
11. Blocker AJ, et al. (2008) What's the point of the type III secretion system needle? *Proc Natl Acad Sci USA* 105:6507–6513.
12. Deane JE, et al. (2006) Molecular model of a type III secretion system needle: Implications for host-cell sensing. *Proc Natl Acad Sci USA* 103:12529–12533.
13. Poyraz O, et al. (2010) Protein refolding is required for assembly of the type three secretion needle. *Nat Struct Mol Biol* 17:788–792.
14. Cordes FS, et al. (2005) Helical packing of needles from functionally altered Shigella type III secretion systems. *J Mol Biol* 354:206–211.
15. Galkin VE, Schmied WH, Schraidt O, Marlovits TC, Egelman EH (2010) The structure of the Salmonella typhimurium type III secretion system needle shows divergence from the flagellar system. *J Mol Biol* 396:1392–1397.
16. Fujii T, Iwane AH, Yanagida T, Namba K (2010) Direct visualization of secondary structures of F-actin by electron cryomicroscopy. *Nature* 467:724–728.
17. Fujii T, Kato T, Namba K (2009) Specific arrangement of alpha-helical coiled coils in the core domain of the bacterial flagellar hook for the universal joint function. *Structure* 17:1485–1493.
18. Wang Y, et al. (2007) Differences in the electrostatic surfaces of the type III secretion needle proteins PrgI, BsaL, and MxiH. *J Mol Biol* 371:1304–1314.
19. Zhang L, Wang Y, Picking WL, Picking WD, De Guzman RN (2006) Solution structure of monomeric BsaL, the type III secretion needle protein of Burkholderia pseudomallei. *J Mol Biol* 359:322–330.
20. Samatey FA, et al. (2004) Structure of the bacterial flagellar hook and implication for the molecular universal joint mechanism. *Nature* 431:1062–1068.
21. Yonekura K, Maki-Yonekura S, Namba K (2003) Complete atomic model of the bacterial flagellar filament by electron cryomicroscopy. *Nature* 424:643–650.
22. Quinaud M, et al. (2007) Structure of the heterotrimeric complex that regulates type III secretion needle formation. *Proc Natl Acad Sci USA* 104:7803–7808.
23. Sun P, Tropea JE, Austin BP, Cherry S, Waugh DS (2008) Structural characterization of the Yersinia pestis type III secretion system needle protein YscF in complex with its heterodimeric chaperone YscE/YscG. *J Mol Biol* 377:819–830.
24. Yonekura K, et al. (2000) The bacterial flagellar cap as the rotary promoter of flagellin self-assembly. *Science* 290:2148–2152.
25. Sory MP, Cornelis GR (1994) Translocation of a hybrid YopE-adenylate cyclase from Yersinia enterocolitica into HeLa cells. *Mol Microbiol* 14:583–594.
26. Sorg I, et al. (2007) YscU recognizes translocators as export substrates of the Yersinia injectisome. *EMBO J* 26:3015–3024.
27. Crepin VF, Shaw R, Abe CM, Knutton S, Frankel G (2005) Polarity of enteropathogenic *Escherichia coli* EspA filament assembly and protein secretion. *J Bacteriol* 187:2881–2889.
28. Iino T (1969) Polarity of flagellar growth in salmonella. *J Gen Microbiol* 56:227–239.
29. Journet L, Agrain C, Broz P, Cornelis GR (2003) The needle length of bacterial injectisomes is determined by a molecular ruler. *Science* 302:1757–1760.
30. Moriya N, Minamino T, Hughes KT, Macnab RM, Namba K (2006) The type III flagellar export specificity switch is dependent on FliK ruler and a molecular clock. *J Mol Biol* 359:466–477.
31. Erhardt M, et al. (2010) The role of the FliK molecular ruler in hook-length control in Salmonella enterica. *Mol Microbiol* 75:1272–1284.
32. Wagner S, et al. (2009) The helical content of the YscP molecular ruler determines the length of the Yersinia injectisome. *Mol Microbiol* 71:692–701.
33. Erhardt M, Singer HM, Wee DH, Keener JP, Hughes KT (2011) An infrequent molecular ruler controls flagellar hook length in Salmonella enterica. *EMBO J* 30:2948–2961.
34. Samatey FA, et al. (2001) Structure of the bacterial flagellar protofilament and implications for a switch for supercoiling. *Nature* 410:331–337.
35. Maki-Yonekura S, Yonekura K, Namba K (2010) Conformational change of flagellin for polymorphic supercoiling of the flagellar filament. *Nat Struct Mol Biol* 17: 417–422.
36. Egelman EH (2000) A robust algorithm for the reconstruction of helical filaments using single-particle methods. *Ultramicroscopy* 85:225–234.